Kovove Mater. 51 2013 311–316
DOI: 10.4149/km_2013_5_311

Crack identification using elastic waves: a boundary element method

N. Flores-Guzmán[1], J. Núñez-Farfán[2], E. Olivera-Villaseñor[2], J. E. Rodríguez-Sánchez[2], C. Ortiz-Alemán[2], M. Orozco-del-Castillo[2], A. Rodríguez-Castellanos[2]*

[1] *Centro de Investigación en Matemáticas, Jalisco s/n, Mineral de Valenciana, Guanajuato, México*
[2] *Instituto Mexicano del Petróleo, Eje Central Lázaro Cárdenas 152, Gustavo A. Madero 07730, México D.F., México*

Received 12 January 2011, received in revised form 1 August 2013, accepted 1 August 2013

Abstract

This work is aimed to obtain numerical results that allow the detection and characterization of subsurface discontinuities in metallic materials by the application of Rayleigh compression and shear elastic waves. The solution is obtained from boundary integral equations, which belong to the field of elasto-dynamics. Subsequent to the implementation of the boundary conditions, a system of Fredholm's integral equation of second kind and zero order is obtained in frequency domain, which is solved using the method of Gaussian elimination. Resonance peaks arise from analysis in frequency domain allowing inferring the presence of discontinuities. Aluminum, copper, steel, molybdenum, titanium and tungsten materials were analyzed, however, a greater emphasis on the steel properties was considered due to its extended use. Results obtained are in agreement with those published in references.

K e y w o r d s: crack detection, elastic waves, Rayleigh's waves, discontinuities, boundary element method

1. Introduction

It is well known that the presence of cracks in structural components can compromise its integrity. Cracks in materials used in mechanical and civil engineering can cause reduction in strength which leads to instability, leakage or collapse depending on the cracked component.

The development of studies for the identification and characterization of cracks has its origins in a variety of areas, citing for example Griffith [1]. The technological progress focused on non-destructive testing (NDT) of materials has led to the development of devices such as pulse generators and receivers that can reach frequencies as high as 200 MHz. On the other hand, advances on theoretical and numerical models [2, 3] have proved to be useful for a joint interpretation with developments in the NDT field [4, 5]. An important overview on theoretical results in relation to the interaction of elastic waves with cracks can be seen in Zhang and Gross [6].

The identification and characterization of subsurface cracks and surface breaking cracks using Rayleigh waves are of much interest in the industry, see for example references [7–12].

This paper considers the study of boundary integral equations, derived from the Somigliana's classical theorem, to deal with the detection and characterization of subsurface discontinuities using elastic waves. Particularly, this method can be seen as one belonging to the boundary element method (BEM), and acquires the character of indirect (IBEM) because the force densities which are unknown in the integrand are obtained in an intermediate step. Subsequent to the implementation of the boundary conditions a system of Fredholm's integral equations of second kind and zero order is obtained in the frequency domain, which is solved using the method of Gaussian elimination. It is important to mention that analysis in frequency domain reveals resonance peaks, which can be linked to the presence of subsurface discontinuities.

*Corresponding author: tel.: + 52 55 91758145; e-mail address: arcastel@imp.mx

2. Boundary integral equation

If anelastic solid domain V bounded by its boundary S is considered, the diffracted displacement and traction fields under harmonic excitation can be expressed, neglecting body forces, by means of the single-layer boundary integral equations:

$$u_i^{\mathrm{d}}(\boldsymbol{x}) = \int_{\partial S} G_{ij}(\boldsymbol{x};\boldsymbol{\xi})\phi_j(\boldsymbol{\xi})\mathrm{d}S_\xi, \tag{1}$$

and

$$t_i^{\mathrm{d}}(\boldsymbol{x}) = c\phi_i(\boldsymbol{x}) + \int_{\partial S} T_{ij}(\boldsymbol{x};\boldsymbol{\xi})\phi_j(\boldsymbol{\xi})\mathrm{d}S_\xi, \tag{2}$$

where $u_i^{\mathrm{d}}(\boldsymbol{x})$ is ith component of the displacement at point $\boldsymbol{x}$, $G_{ij}(\boldsymbol{x};\boldsymbol{\xi})$ is Green's function, which represents the displacement produced in direction i at $\boldsymbol{x}$ due to the application of a unit force in direction j at point $\boldsymbol{\xi}$, $\phi_j(\boldsymbol{\xi})$ is the force density in the direction j at point $\boldsymbol{\xi}$. The product $\phi_j(\boldsymbol{\xi})\mathrm{d}S_\xi$ is the force distribution at the surface S (the subscripts i, j are limited to be 1 or 3). The subscript in the differential shows the variable over which the integration is done. This integral equation can be obtained from Somigliana's representation [13]. Furthermore, it was demonstrated that if $\phi_j(\boldsymbol{\xi})$ is continuous along S, in that case, the displacement field is continuous across S [14]. $t_i^{\mathrm{d}}(\boldsymbol{x})$ is ith component of tractions, $c = 0.5$ if $\boldsymbol{x}$ tends to the boundary S "from inside" the region, $c = -0.5$ if $\boldsymbol{x}$ tends to S "from outside" the region, or $c = 0$ if $\boldsymbol{x}$ is not at S. $T_{ij}(\boldsymbol{x};\boldsymbol{\xi})$ is Green's function traction, i.e., the traction in i direction at point $\boldsymbol{x}$, linked to the unit vector $n_i(\boldsymbol{x})$, due to the application of a unitary force in j direction at $\boldsymbol{\xi}$ on S. The following section presents Green's functions for displacements and tractions.

3. Two-dimensional Green's functions in unbounded space

In a homogeneous isotropic elastic unbounded medium, 2D Green's functions are the displacements and tractions responses of the medium at a given location $\boldsymbol{x}$ when a unit line load is applied at $\boldsymbol{\xi}$.

Assuming harmonic time dependence $\exp(\mathrm{i}\omega t)$, where $\mathrm{i} = \sqrt{-1}$, ω is circular frequency, and t is time, the displacement in i direction, when the load is applied in j direction, can be expressed as:

$$G_{ij}(\boldsymbol{x};\boldsymbol{\xi}) = A\delta_{ij} - B(2\gamma_i\gamma_j - \delta_{ij}). \tag{3}$$

On the other hand, the tractions at $\boldsymbol{x}$ in i direction for a given unit vector n_i normal to S when the unit load is applied at $\boldsymbol{\xi}$ in the direction j are:

$$T_{ij} = \frac{\mu}{r}\left\{\left[-4B + \lambda\frac{D(\omega r/\alpha)}{2\mu\alpha^2}\right]\gamma_j n_i + \right.$$
$$\left. + \left[-4B + \frac{D(\omega r/\beta)}{2\beta^2}\right]\times\left[\gamma_i n_j + \gamma_k n_k\delta_{ij}\right]\right\} +$$
$$+ \frac{\mu}{r}\left\{(C + 16B)\,\gamma_i\gamma_j\gamma_k n_k\right\}. \tag{4}$$

For Eqs. (3) and (4) these expressions are defined:

$$A = \frac{1}{\mathrm{i}8\rho}\left[\frac{H_0^{(2)}(\omega r/\alpha)}{\alpha^2} + \frac{H_0^{(2)}(\omega r/\beta)}{\beta^2}\right], \tag{5}$$

$$B = \frac{1}{\mathrm{i}8\rho}\left[\frac{H_2^{(2)}(\omega r/\alpha)}{\alpha^2} - \frac{H_2^{(2)}(\omega r/\beta)}{\beta^2}\right], \tag{6}$$

$$C = \frac{D(\omega r/\alpha)}{\alpha^2} - \frac{D(\omega r/\beta)}{\beta^2}, \tag{7}$$

$$D(p) = \frac{\mathrm{i}}{2\rho}pH_1^{(2)}(p), \tag{8}$$

where λ and μ are the Lamé's constants, ρ is mass density, $\alpha = \sqrt{(\lambda+2\mu)/\rho}$ and $\beta = \sqrt{\mu/\rho}$ are the P and S wave velocities, respectively, $r = \sqrt{(x_1-\xi_1)^2 + (x_3-\xi_3)^2}$, $\gamma_j = (x_j - \xi_j)/r$, δ_{ij} is Kronecker's delta ($= 1$ if $i = j$, $= 0$ if $i \neq j$) and $H_m^{(2)}(\cdot)$ is the Hankel's function of second kind and order m.

4. Statement of the problem

In general terms, the response of a cracked medium should satisfy the displacement and traction states represented by the sum of a free field (super index "o") and a diffracted field (super index "d"), this is: $u_i(\boldsymbol{x}) = u_i^{\mathrm{o}}(\boldsymbol{x}) + u_i^{\mathrm{d}}(\boldsymbol{x})$ and $t_i(\boldsymbol{x}) = t_i^{\mathrm{o}}(\boldsymbol{x}) + t_i^{\mathrm{d}}(\boldsymbol{x})$, respectively. The free field always represents the incidence of Rayleigh, compressional (P) or shear (SV) waves. To represent the crack or discontinuity, tractions free boundary conditions must be established at its contour, i.e., $t_i(\boldsymbol{x}) = 0$.

The integral equations established in Eqs. (1) and (2) allow the inclusion of cracks or discontinuities, because of the use of multi-region concept, in which the domain of study may be discrete in regions and the joint between them is given by the boundary conditions that represent continuity ($u_i^{\mathrm{R}}(\boldsymbol{x}) = u_i^{\mathrm{E}}(\boldsymbol{x})$ and $t_i^{\mathrm{R}}(\boldsymbol{x}) = t_i^{\mathrm{E}}(\boldsymbol{x})$), e.g., for the union of the region R and the region E. To include a crack or discontinuity between two regions, traction-free boundary conditions $t_i^{\mathrm{R}}(\boldsymbol{x}) = 0$ and $t_i^{\mathrm{E}}(\boldsymbol{x}) = 0$ must be established for the discontinuity sides that belong to each region.

Each surface is divided into boundary elements of length equal to or less than 1/6 of the shortest SV wavelength each, depending on the frequency. For example, for a free surface, the joint between regions R and E and the discontinuity requires N, M and K boundary elements, respectively, then Eqs. (1) and (2) must be written, considering free and diffracted fields and boundary conditions described previously, as:

$$c\phi_i^{\mathrm{R}}(\boldsymbol{x}) + \int_{\partial \mathrm{R}} \phi_j^{\mathrm{R}}(\boldsymbol{\xi})\, T_{ij}^{\mathrm{R}}(\boldsymbol{x};\boldsymbol{\xi})\, \mathrm{d}S_\xi = -t_i^{\mathrm{oR}}(\boldsymbol{x}), \quad \boldsymbol{x} \in \partial_3 \mathrm{R}, \tag{9}$$

$$\int_{\partial \mathrm{R}} \phi_j^{\mathrm{R}}(\boldsymbol{\xi})\, G_{ij}^{\mathrm{R}}(\boldsymbol{x};\boldsymbol{\xi})\, \mathrm{d}S_\xi - \int_{\partial \mathrm{E}} \phi_j^{\mathrm{E}}(\boldsymbol{\xi})\, G_{ij}^{\mathrm{E}}(\boldsymbol{x};\boldsymbol{\xi})\, \mathrm{d}S_\xi = u_i^{\mathrm{oE}}(\boldsymbol{x}) - u_i^{\mathrm{oR}}(\boldsymbol{x}), \quad \boldsymbol{x} \in \partial_1 \mathrm{R} = \partial_1 \mathrm{E}, \tag{10}$$

$$c\phi_i^{\mathrm{R}}(\boldsymbol{x}) + \int_{\partial \mathrm{R}} \phi_j^{\mathrm{R}}(\boldsymbol{\xi})\, T_{ij}^{\mathrm{R}}(\boldsymbol{x};\boldsymbol{\xi})\, \mathrm{d}S_\xi - c\phi_i^{\mathrm{E}}(\boldsymbol{x}) - \int_{\partial \mathrm{E}} \phi_j^{\mathrm{E}}(\boldsymbol{\xi})\, T_{ij}^{\mathrm{E}}(\boldsymbol{x};\boldsymbol{\xi})\, \mathrm{d}S_\xi = t_i^{\mathrm{oE}}(\boldsymbol{x}) - t_i^{\mathrm{oR}}(\boldsymbol{x}), \quad \boldsymbol{x} \in \partial_1 \mathrm{R} = \partial_1 \mathrm{E}, \tag{11}$$

$$c\phi_i^{\mathrm{R}}(\boldsymbol{x}) + \int_{\partial \mathrm{R}} \phi_j^{\mathrm{R}}(\boldsymbol{\xi})\, T_{ij}^{\mathrm{R}}(\boldsymbol{x};\boldsymbol{\xi})\, \mathrm{d}S_\xi = -t_i^{\mathrm{oR}}(\boldsymbol{x}), \quad \boldsymbol{x} \in \partial_2 \mathrm{R}, \tag{12}$$

and

$$c\phi_i^{\mathrm{E}}(\boldsymbol{x}) + \int_{\partial \mathrm{E}} \phi_j^{\mathrm{E}}(\boldsymbol{\xi})\, T_{ij}^{\mathrm{E}}(\boldsymbol{x};\boldsymbol{\xi})\, \mathrm{d}S_\xi = -t_i^{\mathrm{oE}}(\boldsymbol{x}), \quad \boldsymbol{x} \in \partial_2 E. \tag{13}$$

Region R is formed by the boundary $\partial R = \partial_1 R \cup \partial_2 R \cup \partial_3 R$, while the region E by the boundary $\partial E = \partial_1 E \cup \partial_2 E$. $\partial_1 R$ and $\partial_1 E$ represent the continuous segments between region R and E, $\partial_2 R$ is the discontinuity or crack face on the side of the region R, $\partial_2 E$ is the discontinuity or crack face on the side of the region E, and $\partial_3 R$ is the free surface belonging to region R.

Equations (9) to (13) form Fredholm's system of integral equations to be solved. Once the unknown values (ϕ's) are obtained, the diffracted displacement and traction fields are computed by means of Eqs. (1) and (2), respectively.

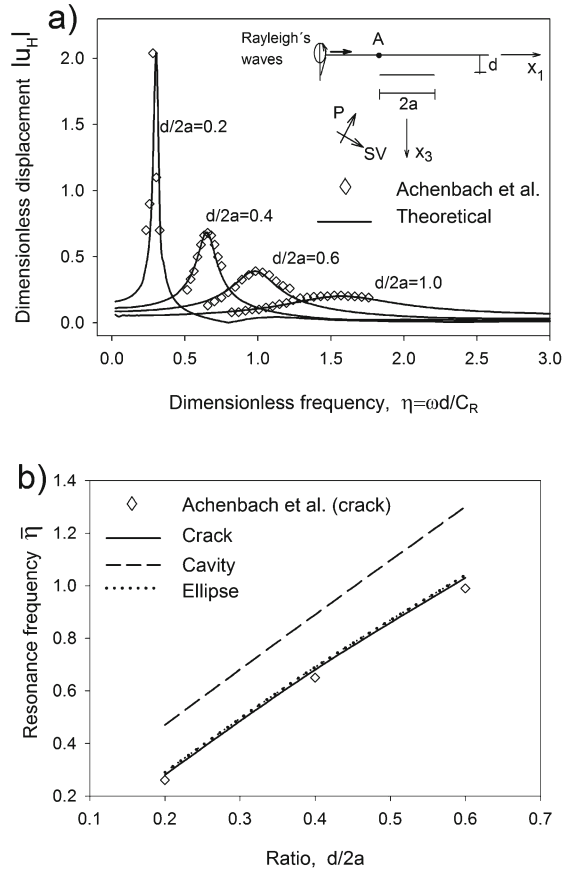

Fig. 1. a) Dimensionless horizontal displacements for four crack depths at site A, b) resonance frequencies versus depth relations for three shape defects.

5. Validation and numerical examples

Two references have been selected to validate the results obtained by this formulation, the first is Achenbach et al. [3], and the other is Graff [15]. Achenbach et al. studied the behavior of cracks under the incidence of P waves and described the behavior for four depth ratios $d/2a = 0.2$, 0.4, 0.6 and 1.0, where d is crack depth and $2a$ is crack length, Figure 1a shows the dimensionless horizontal displacements calculated at point A.

Achenbach et al. also carried out dimensionless frequency analysis for the range $0 \leq \eta \leq 3.0$, where $\eta = \omega d/C_{\mathrm{R}}$, ω is the circular frequency, and C_{R} represents the Rayleigh's wave velocity. From Fig. 1a it can be observed that theoretical results obtained by the formulation introduced in this work are in good agreement with Achenbach et al. Figure 1b illustrates the resonance frequencies versus $d/2a$ ratios for subsurface cracks, elliptical defects ($b = 0.2a$) and cavities (radius $= a$) obtained from the formulation introduced in this work, there can also be seen good agreement with Achenbach et al. Figure 1b also allows a com-

Table 1. Elastic constants of the metallic materials studied

Material	ρ (mg m^{-3})	α (km s^{-1})	β (km s^{-1})	E (GPa)	ν	λ (g Pa^{-1})	μ (g Pa^{-1})
Aluminum	2.70	6.42	3.04	67.60	0.35	61.30	24.90
Copper	8.93	5.01	2.27	126.00	0.37	132.00	46.00
Molybdenum	10.00	6.30	3.40	299.00	0.29	165.00	115.00
Steel	7.89	5.79	3.10	196.00	0.29	112.00	75.80
Titanium carbide	5.15	8.27	5.16	323.00	0.18	77.90	137.00
Tungsten	19.40	5.20	2.90	415.00	0.27	198.00	163.00

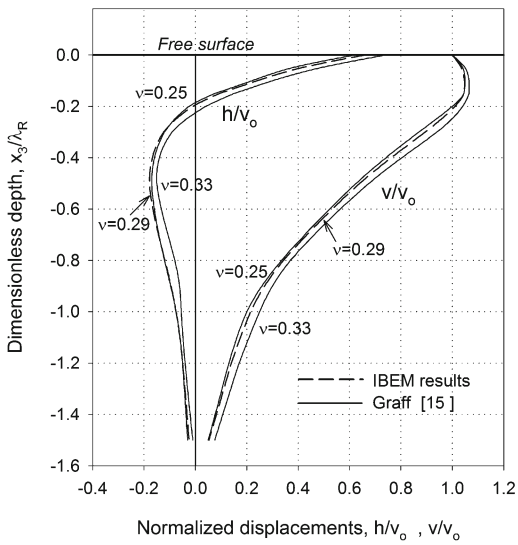

Fig. 2. Horizontal and vertical displacements normalized with the vertical displacement value at the surface (v_o) for three Poisson's ratios.

parison of defect shape, depth and size based on a frequency analysis.

Characterizing the presence of subsurface cracks by the incidence of Rayleigh's waves, the typical curve of horizontal and vertical displacements normalized with v_o can be observed from Fig. 2, which is the value for the vertical displacement at the surface. The influence depth of Rayleigh's waves for a non cracked medium is a Rayleigh's wavelength, where λ_R is the Rayleigh's wavelength for a given frequency. These typical curves are plotted for three Poisson's ratios $\nu = 0.25$, 0.29 and 0.33, the dashed line shows results obtained by IBEM. Poisson's ratio $\nu = 0.29$ corresponds to steel, see Table 1, good agreement can be observed from IBEM and Graff's results [15].

For steel $\nu = 0.29$ in the frequency range $0 \leq \eta \leq 3.0$, horizontal and vertical displacement fields are shown in Figs. 3a, and 3b, respectively, for the shallowest ($d/2a = 0.2$) and deepest ($d/2a = 1.0$) crack ratios. It is expected that a shallow crack causes major alterations to Rayleigh's wave front, while a deep crack has an effect almost negligible for both displacements.

Figure 3c shows a spectral ratio h/v almost constant, except for crack depths $d/2a = 0.2$ and $d/2a = 0.4$, for other crack depths h/v is almost constant. In an enlarged detail of Fig. 3c the first peak caused by crack depth $d/2a = 0.2$ can be observed, as well as the constant behavior shown for crack depth $d/2a = 1.0$, additionally it can be seen that at low frequencies the spectral ratio h/v tends to 0.66 for any crack depth, however, this value is maintained even for the case when there is no crack, see Fig. 2 for $h = 0.66$ and $v = 1.00$ values on the surface, then $h/v = 0.66$.

To study the influence of cracks under the incidence of shear elastic waves (S) located at depth ratios $d/2a = 0.2$, 0.4, 0.6 and 1.0, Figs. 4a,b show horizontal and vertical displacements, respectively, versus dimensionless frequency range $0 \leq \eta \leq 3.0$. Again, it is noted that the shallow crack $d/2a = 0.2$ causes a greater alteration on the SV wave front and presents more acute resonance peaks. Moreover, for deeper cracks $d/2a = 0.6$ and 1.0, the response measured at point A shown in Fig. 1 tends to be negligible.

Finally, a group of metallic materials shown in Table 1 has been selected to display the frequencies at which resonance effects arise. Propagation velocities employed for the analysis as well as their densities and Poisson's ratios can be consulted in [16]. Figure 5 shows the resonance frequencies obtained for a crack embedded in the materials of Table 1, with length $2a = 1$ cm and depth $d = 0.2$ cm this is $d/2a = 0.2$. Results obtained by the formulation introduced in this work are drawn with dashed line. It is important to mention that to verify these resonance frequencies for the materials shown in Table 1, two additional results have been included in Fig. 5 obtained by the finite element method (FEM) using the ANSYS software package. The space between the up crack face and the free surface was idealized as a beam considering two extreme boundary conditions, described as follows. First, continuous line represents the response as a beam rigidly supported at its ends, FEM (model 1) with length $2a = 1$ cm and height 0.2 cm. Second, dotted line represents the same beam but simply supported at its ends, FEM (model 2). The curve obtained by the formulation introduced in this work by IBEM is located between the FEM curves. Additionally, Fig. 5 shows a shaded area to

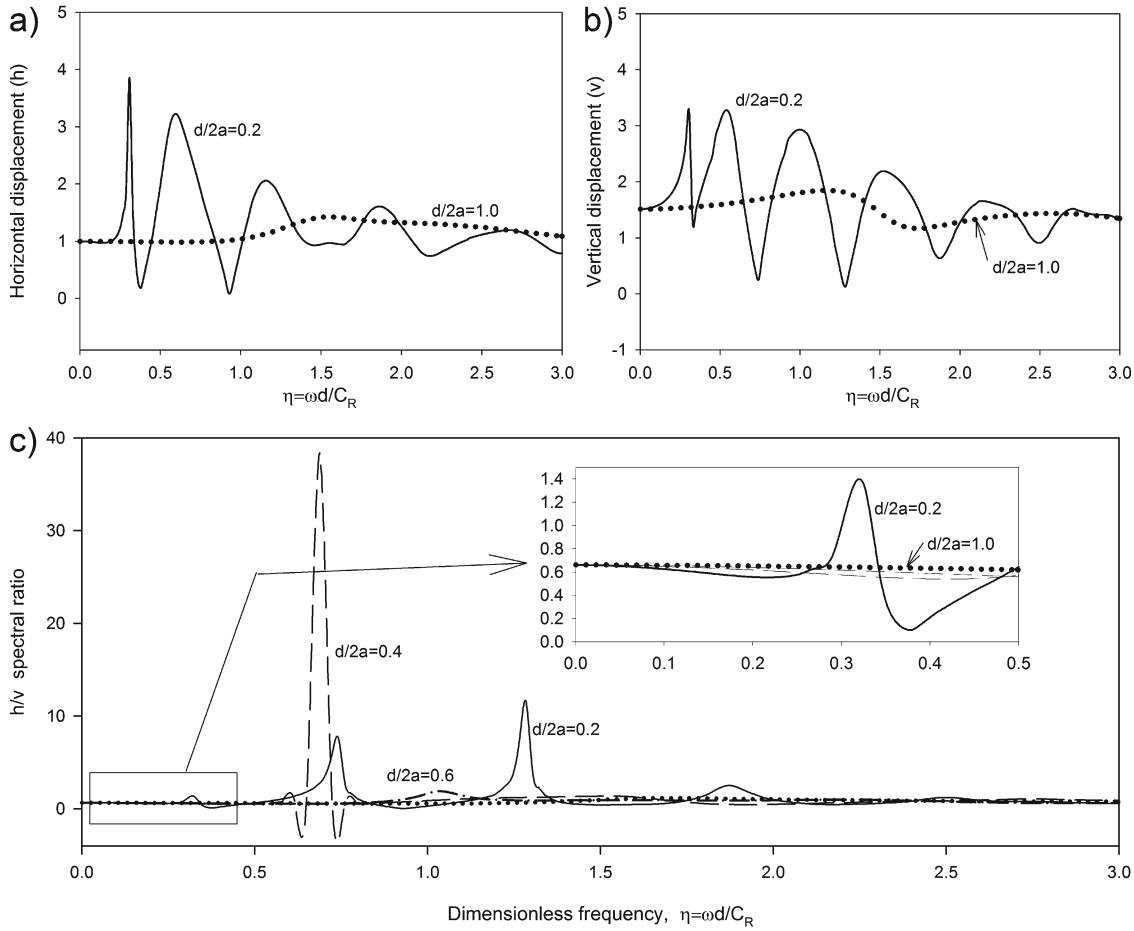

Fig. 3. Cracks subjected to the incidence of Rayleigh's waves: a) horizontal displacements for crack depth ratios $d/2a = 0.2$ and $d/2a = 1.0$, b) vertical displacements for crack depth ratios $d/2a = 0.2$ and $d/2a = 1.0$, c) spectral ratio h/v for crack depths $d/2a = 0.2$, 0.4, 0.6 and 1.0.

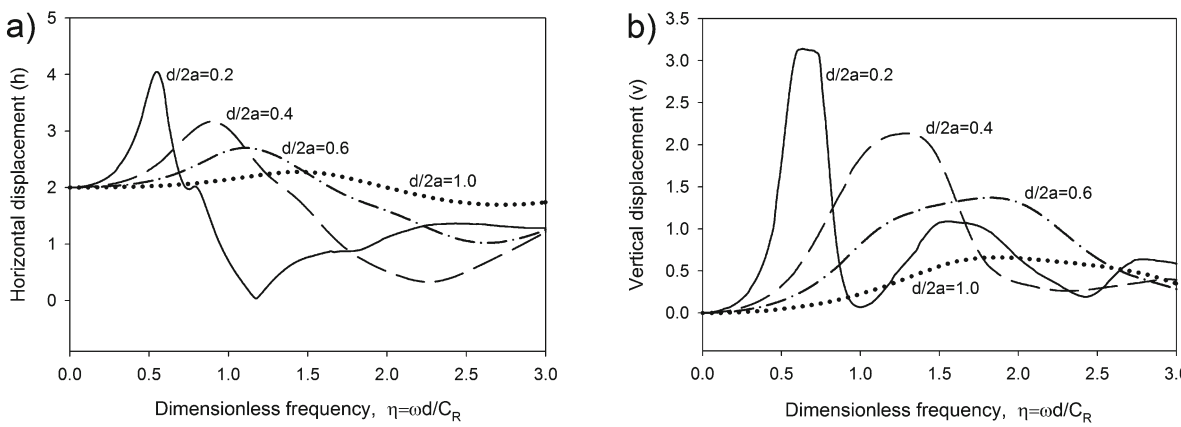

Fig. 4. Cracks subjected to the incidence of S waves: a) horizontal displacements, b) vertical displacements.

highlight the value of the dynamic shear modulus that characterizes the metallic material used, according to Table 1. Similar curves to this one can be developed for other crack depths ($d/2a = 0.4$, 0.6 and 1.0).

6. Conclusions

The present work was derived from the Fredholm's integral equations of the second kind and zero order. After the implementation of the boundary condi-

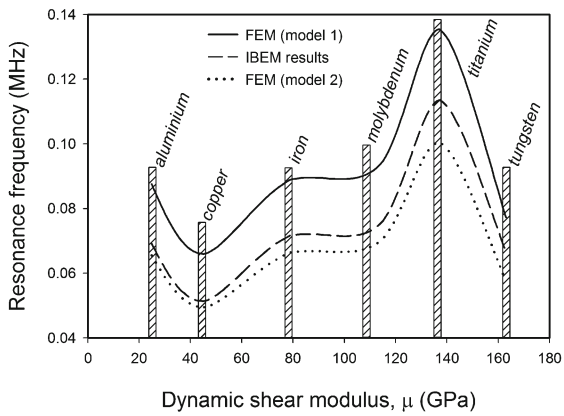

Fig. 5. Resonance frequencies versus dynamic shear modulus for $d/2a = 0.2$ by FEM and IBEM analysis.

tions and the use of the multiregional concept, it was possible to formulate a system of integral equations, where the unknowns named as force densities were obtained. This method is understood as an indirect boundary element formulation or IBEM and can be seen as a conceptualization of Somigliana's classical theorem.

The excitation of the system was carried out by the incidence of Rayleigh, P and S waves leading to spectrum that is useful for the characterization of embedded cracks in materials, particularly in the metallic materials studied in this work.

The results obtained in the present work were validated with published results of Achenbach et al. [3] and Graff [15], and also by means of the finite element method. The presence of cracks or discontinuities causes resonance peaks, which can be identified using frequency analysis, the resonance peaks are sharper as the defects are shallower.

References

[1] Griffith, A. A.: Philosophical Transactions of Royal Society of London, *A221*, 1921, p. 163. doi:10.1098/rsta.1921.0006

[2] Freund, L. B.: Journal of Mechanics and Physics of Solids, *21*, 1972, p. 47. doi:10.1016/0022-5096(73)90029-X

[3] Achenbach, J. D., Angel, Y. C., Lin, W.: In: Wave Propagation in Homogeneous Media and Ultrasonic Nondestructive Evaluation. Ed.: Johnson, G. C. New York, American Society of Mechanical Engineers 1984.

[4] Bray, D. E., Stanley, R. K.: Nondestructive Evaluation, a Tool in Design, Manufacturing and Service. Boca Raton, FLA, CRC Press 1997.

[5] Scales, J., Wijk, K. V.: Applied Physics Letters, *74*, 1999, p. 3899. doi:10.1063/1.124217

[6] Zhang, C. H., Gross, D.: On Wave Propagation in Elastic Solids with Cracks. Southampton, UK, Computational Mechanics Publications 1998.

[7] Tweddell, W. R.: Materials Evaluation, *48*, 1990, p. 1348.

[8] Van Derkolk, C. M., Guest, W. S., Potters, J. H. H. M.: Geophysical Prospecting, *49*, 2001, p. 179. doi:10.1046/j.1365-2478.2001.00250.x

[9] Ochiai, M., Lévesque, D., Talbot, R., Blouin, A., Fukumoto, A., Monchalin, J. P.: Materials Evaluation, *62*, 2004, p. 450.

[10] Masserey, B., Mazza, E.: Journal of the Acoustical Society of America, *118*, 2005, p. 3585. doi:10.1121/1.2109407

[11] Masserey, B., Aebi, L., Mazza, E.: Ultrasonics, *44*, SUPPL., 2006, p. e957. PMid:16797633. doi:10.1016/j.ultras.2006.05.059

[12] Na, J. K., Blackshire, J. L.: NDT and E International, *43*, 2010, p. 432. doi:10.1016/j.ndteint.2010.04.003

[13] Sánchez-Sesma, F. J., Campillo, M.: Bulletin of the Seismological Society of America, *81*, 1991, p. 1.

[14] Kupradze, V. D.: Dynamical problems in elasticity. In: Progress in Solid Mechanics. Eds.: Sneddon, I. N., Hill, R. Amsterdam, North-Holland 1963.

[15] Graff, K. F.: Wave Motion in Elastic Solids. Columbus, OH, Ohio State University Press 1975. PMCid:PMC1775921

[16] Bedford, A., Drumheller, D. S.: Introduction to Elastic Wave Propagation. New York, John Wiley & Sons 1994.